Research Article | Vol. 24, No. 22 | 31 Oct 2016 | OPTICS EXPRESS A1408

Optics EXPRESS

Effective medium analysis of absorption enhancement in short-pitch metal grating incorporated organic solar cells

YE ZHANG,[1] YANXIA CUI,[1,2,4] WENYAN WANG,[1] KIN HUNG FUNG,[3] TING JI,[1] YUYING HAO,[1,5] AND FURONG ZHU[2]

[1]*Key Lab of Advanced Transducers and Intelligent Control System of Ministry of Education, College of Physics and Optoelectronics, Taiyuan University of Technology, Taiyuan 030024, China*
[2]*Department of Physics and Institute of Advanced Materials, Hong Kong Baptist University, Kowloon Tong, Hong Kong*
[3]*Department of Applied Physics, The Hong Kong Polytechnic University, Hong Kong*
[4]*yanxiacui@gmail.com,*
[5]*haoyuying@tyut.edu.cn*

Abstract: The effective medium theory is applied to analyze the absorption enhancement in organic solar cells with a short-pitch metal grating. A 37% improvement in the absorption of the active layer is achieved with respect to that of a planar control cell. It is inspired that the propagating surface plasmon modes are excited at the interface between the effective medium layer and the flat metal plate, resulting in a reduction of light reflection. In real structure, the electric field redistributes with its intensity in the region with active materials infiltrated in the grooves increases significantly, exhibiting like hot spots to assist in achieving broadband absorption enhancement. Moreover, the localized surface plasmon resonances excited at the top of the metal ridges also contribute to the absorption enhancement in the cells.

OCIS codes: (160.1190) Anisotropic optical materials; (010.1030) Absorption; (050.2065) Effective medium theory; (350.6050) Solar energy.

References and links

1. S. Günes, H. Neugebauer, and N. S. Sariciftci, "Conjugated polymer-based organic solar cells," Chem. Rev. **107**(4), 1324–1338 (2007).
2. G. Li, V. Shrotriya, J. Huang, Y. Yao, T. Moriarty, K. Emery, and Y. Yang, "High-efficiency solution processable polymer photovoltaic cells by self-organization of polymer blends," Nat. Mater. **4**(11), 864–868 (2005).
3. Z. H. Wu, B. Wu, H. L. Tam, and F. R. Zhu, "An insight on oxide interlayer in organic solar cells: From light absorption and charge collection perspectives," Org. Electron. **31**, 266–272 (2016).
4. S. Nagamani, G. Kumarasamy, M. Song, C. S. Kim, D.-H. Kim, S. Y. Ryu, J.-W. Kang, and S.-H. Jin, "Optical absorption and electrical properties of enhanced efficiency in organic solar cells as interfacial layer with Au NPs," Synth. Met. **217**, 117–122 (2016).
5. X. Tian, Y. Zhang, Y. Hao, Y. Cui, W. Wang, F. Shi, H. Wang, B. Wei, and W. Huang, "Semitransparent inverted organic solar cell with improved absorption and reasonable transparency perception based on the nanopatterned MoO3/Ag/MoO3 anode," J. Nanophotonics **9**(1), 093043 (2015).
6. A. Williamson, É. McClean, D. Leipold, D. Zerulla, and E. Runge, "The design of efficient surface-plasmon-enhanced ultra-thin polymer-based solar cells," Appl. Phys. Lett. **99**(9), 093307 (2011).
7. M. A. Sefunc, A. K. Okyay, and H. V. Demir, "Plasmonic backcontact grating for P3HT:PCBM organic solar cells enabling strong optical absorption increased in all polarizations," Opt. Express **19**(15), 14200–14209 (2011).
8. R. Lampande, G. W. Kim, M. J. Park, B. Y. Kang, and J. H. Kwon, "Efficient light harvesting in inverted polymer solar cells using polymeric 2D-microstructures," Sol. Energy Mater. Sol. Cells **151**, 162–168 (2016).
9. W. C. Choy and X. Ren, "Plasmon-electrical effects on organic solar cells by incorporation of metal nanostructures," IEEE J. Sel. Top. Quantum Electron. **22**(1), 1–9 (2016).
10. W. E. Sha, X. Li, and W. C. Choy, "Breaking the space charge limit in organic solar cells by a novel plasmonic-electrical concept," Sci. Rep. **4**, 6236 (2014).
11. A. Baba, N. Aoki, K. Shinbo, K. Kato, and F. Kaneko, "Grating-coupled surface plasmon enhanced short-circuit current in organic thin-film photovoltaic cells," ACS Appl. Mater. Interfaces **3**(6), 2080–2084 (2011).

#272937 http://dx.doi.org/10.1364/OE.24.0A1408
Journal © 2016 Received 1 Aug 2016; revised 2 Sep 2016; accepted 14 Sep 2016; published 22 Sep 2016

Optics EXPRESS

12. Y. Cui, Y. He, Y. Jin, F. Ding, L. Yang, Y. Ye, S. Zhong, Y. Lin, and S. He, "Plasmonic and metamaterial structures as electromagnetic absorbers," Laser Photonics Rev. **8**(4), 495–520 (2014).
13. Z. Zhou, Z. Zhao, Y. Yu, B. Ai, H. Möhwald, R. C. Chiechi, J. K. Yang, and G. Zhang, "From 1D to 3D: Tunable Sub-10 nm Gaps in Large Area Devices," Adv. Mater. **28**(15), 2956–2963 (2016).
14. Z. Huang, G. Meng, B. Chen, C. Zhu, F. Han, X. Hu, and X. Wang, "Surface-enhanced Raman scattering from au-nanorod arrays with sub-5-nm gaps stuck out of an AAO template," J. Nanosci. Nanotechnol. **16**(1), 934–938 (2016).
15. Y. Bourgin, D. Voigt, T. Käsebier, E.-B. Kley, and U. D. Zeitner, "Periodic sub-100nm structures fabricated by proximity i-line mask-aligner lithography (and self-aligned double patterning)," in *SPIE Advanced Lithography* (ISOP, 2016), pp. 978014–978017.
16. H. H. Wang, C. Y. Liu, S. B. Wu, N. W. Liu, C. Y. Peng, T. H. Chan, C. F. Hsu, J. K. Wang, and Y. L. Wang, "Highly raman-enhancing substrates based on silver nanoparticle arrays with tunable sub-10 nm gaps," Adv. Mater. **18**(4), 491–495 (2006).
17. W. Wang, Y. Hao, Y. Cui, X. Tian, Y. Zhang, H. Wang, F. Shi, B. Wei, and W. Huang, "High-efficiency, broad-band and wide-angle optical absorption in ultra-thin organic photovoltaic devices," Opt. Express **22**(S2), A376–A385 (2014).
18. Y. Zhang, Y. Cui, W. Wang, K. H. Fung, T. Ji, Y. Hao, and F. R. Zhu, "Absorption enhancement in organic solar cells with a built-in short-pitch plasmonic grating," Plasmonics **10**(4), 773–781 (2015).
19. S. Tang, Y. Fang, Z. Liu, L. Zhou, and Y. Mei, "Tubular optical microcavities of indefinite medium for sensitive liquid refractometers," Lab Chip **16**(1), 182–187 (2016).
20. W. Khunsin, J. Dorfmüller, M. Esslinger, R. Vogelgesang, C. Rockstuhl, C. Etrich, and K. Kern, "Quantitative and direct near-field analysis of plasmonic-induced transparency and the observation of a plasmonic breathing mode," ACS Nano **10**(2), 2214–2224 (2016).
21. Z. X. Chen, Z. G. Chen, Y. Ming, Y. Wu, and Y. Q. Lu, "Tunable waveguide bends with graphene-based anisotropic metamaterials," Appl. Phys. Express **9**(2), 025101 (2016).
22. T. Abhilash, M. Balasubrahmaniyam, and S. Kasiviswanathan, "Effective medium based optical analysis with finite element method simulations to study photochromic transitions in Ag-TiO2 nanocomposite films," J. Appl. Phys. **119**(12), 123104 (2016).
23. G. Haidari, M. Hajimahmoodzadeh, H. R. Fallah, and M. G. Varnamkhasti, "Effective medium analysis of thermally evaporated Ag nanoparticle films for plasmonic enhancement in organic solar cell," Superlattices Microstruct. **85**, 294–304 (2015).
24. Y. Cui, K. H. Fung, J. Xu, H. Ma, Y. Jin, S. He, and N. X. Fang, "Ultrabroadband light absorption by a sawtooth anisotropic metamaterial slab," Nano Lett. **12**(3), 1443–1447 (2012).
25. T. C. Choy, *Effective Medium Theory: Principles and Applications* (Oxford University Press, 2015).
26. E. D. Palik, *Handbook of Optical Constants of Solids* (Academic Press, 1998).
27. W. Wang, Y. Cui, Y. He, Y. Hao, Y. Lin, X. Tian, T. Ji, and S. He, "Efficient multiband absorber based on one-dimensional periodic metal-dielectric photonic crystal with a reflective substrate," Opt. Lett. **39**(2), 331–334 (2014).
28. X. Z. Wang, C. X. Zhao, G. Xu, Z. K. Chen, and F. R. Zhu, "Degradation mechanisms in organic solar cells: localized moisture encroachment and cathode reaction," Sol. Energy Mater. Sol. Cells **104**, 1–6 (2012).
29. B. Wu, Z. H. Wu, H. L. Tam, and F. R. Zhu, "Contrary interfacial exciton dissociation at metal/organic interface in regular and reverse configuration organic solar cells," Appl. Phys. Lett. **105**(10), 103302 (2014).
30. B. Wu, Z. Wu, Q. Yang, F. Zhu, T. W. Ng, C. S. Lee, S. H. Cheung, and S. K. So, "Improvement of charge collection and performance reproducibility in inverted organic solar cells by suppression of ZnO subgap states," ACS Appl. Mater. Interfaces **8**(23), 14717–14724 (2016).
31. W. X. Lan, Y. Cui, Q. Y. Yang, M. F. Lo, C. S. Lee, and F. R. Zhu, "Broadband light absorption enhancement in moth's eye nanostructured organic solar cells," AIP Adv. **5**(5), 057164 (2015).

1. Introduction

Bulk heterojunction organic solar cells (OSCs) have attracted wide interest in recent years because of their evident advantages of light-weight, good flexibility, huge materials varieties and solution fabrication processes at low cost [1, 2]. Significant progress in the power conversion efficiency (PCE) and the stability of OSCs is needed before they become a viable photovoltaic option for commercialization. The absorption in OSCs is limited due to the mismatch between the absorption depth and charge diffusion length, caused by the poor carrier mobility in the organic semiconductors [3, 4]. One feasible approach to boost light absorption, thereby improving the performance of OSCs, is to incorporate some light trapping elements in the active layer without increasing its thickness. So far, metal grating has been popularly adopted in OSCs, bringing forward improved light absorption in the active layer. Theoretical calculations [5–7] indicate that light absorption enhancement in metal grating-incorporated OSCs is due to the existence of plasmonic modes and/or photonic modes.

Optics EXPRESS

Meanwhile, obvious enhancements in PCE of the metal grating-incorporated OSCs has also been successfully demonstrated in experiment [8–11].

Metal gratings with different periodicities exhibit distinct resonances, and the corresponding capabilities of trapping light vary considerably [12]. The performance of metal grating-incorporated OSCs having the grating scale of a few hundred of nanometers has been widely investigated by theoretical simulation, experimental optimization or their combination. With the development of nanofabrication technology including the emergences of the nano-imprinting technology, self-assembling technique, etc., metal gratings with sub-hundred nanometers can be easily realized, e.g., already widely applied in surface-enhanced Raman spectroscopy analyses [13–16]. Our previous works have attempted to introduce the short-pitch metal grating (i.e., in scale of sub-hundred nanometers) into OSCs with either thin or thick active layer [17, 18]. It was found that the absorption enhancement factor produced by the short-pitch metal grating could be much greater than that yielded by the metal grating with period in the scale of a few hundred of nanometers. We attributed the absorption enhancement to the strong localized electric field excited within the nanometer-sized groove, also known as hot spots, after carefully looking into the field distributions at different wavelengths. While it is usually believed that local field enhancement could be very sensitive to the details of the nanostructures, here we show that the results can be reproduced using the effective medium theory [19–24], which means that the performance of our design could still be reached even if there are small fabrication errors. It is anticipated that the effective medium theory can provide an insight on understanding light absorption enhancement in the active layer, which underpins the high efficiency OSCs.

This work reports a theoretical study on elucidating the effect of the short-pitch metal grating on absorption enhancement in OSCs using effective medium theory. Section 2 presents the effective medium theory, based on which a one-dimensional optical lattice can be modeled as an anisotropic material. Section 3 describes the investigated problem and the adopted numerical method. Section 4 analyzes the mechanism of absorption enhancement based on the effective medium theory and an agreement of absorption spectra before and after the equivalent approximation is demonstrated. Section 5 discusses the geometrical conditions when the effective medium approximation is valid, with the grating width, height, and period along with the thickness of the active layer under consideration. The results of this study are summarized in section 6.

2. Effective medium theory

Effective medium theory, *e.g.*, an approximation of a homogeneous medium with effective constitutive parameters of permittivity (ε_{eff}) and permeability (μ_{eff}), is often used to study the optical properties of a complex inhomogeneous material. Effective medium theory can also be applied to OSCs when the size of inhomogeneity features is much smaller than the wavelength of the electromagnetic waves. For example, the buffer layer in OSCs having randomly distributed evaporated Ag nanoparticles was modeled as an effective homogeneous medium with uniform optical properties across the region, yielding agreement with the experimental results [23]. Considering a one-dimensional periodic structure, for example, the effective medium is a good approximation for the active region in the grating OSCs if the lattice pitch is much smaller than the wavelength of the incident light. For OSCs with a short-pitch metal grating [17], a uniform distribution of magnetic field is observed across the geometrically-uneven region, reflecting the effectiveness of effective medium theory for application in this system. In our case, a one-dimensional metal grating is introduced into the OSCs, resulting in an interspersed region including both metal and the active material. The details of the structure are given in Section 3. The interspersed region is modeled as an effective medium, as the lattice pitch is much smaller than the wavelength of the incident light. Then, the problem is to get the effective parameters of the alternating plates made of

Optics EXPRESS

two different materials with relative permittivities of ε_1 and ε_2, and thicknesses of d_1 and d_2, respectively. For a structure comprising of non-magnetic substances, the effective permittivity must fulfill the equation [25]

$$\langle D\rangle = \varepsilon_0 \varepsilon_{\text{eff}} \langle E\rangle. \tag{1}$$

where $\langle D\rangle$ and $\langle E\rangle$ are the spatial average displacement field and electric field, sometimes a weighting function is included in the spatial average. According to the quasi-static limit, the directions parallel and perpendicular to the pates have different effective permittivities ($\varepsilon_{\text{eff}}^{\square}, \varepsilon_{\text{eff}}^{\perp}$) [25]; in other words, the effective medium exhibits the anisotropic material property. That is $\varepsilon_{\text{eff}}^{\square} = \langle D_{\square}\rangle / \langle E_{\square}\rangle$ and $\varepsilon_{\text{eff}}^{\perp} = \langle D_{\perp}\rangle / \langle E_{\perp}\rangle$, where the subscripts "$\square$" and "$\perp$" represent the components parallel and perpendicular to the interfaces between layers, respectively. Using the boundary condition that $E_{\square}$ is continuous and by averaging the displacement field $D_{\square}$ by volume, we get [25]

$$\varepsilon_{\text{eff}}^{\square} = \frac{d_1}{d_1 + d_2}\varepsilon_1 + \frac{d_2}{d_1 + d_2}\varepsilon_2. \tag{2}$$

Similarly, using the boundary condition that $D_{\perp}$ is continuous and by averaging the electric field $E_{\perp}$ by volume, we get

$$\frac{1}{\varepsilon_{\text{eff}}^{\perp}} = \frac{d_1}{d_1 + d_2}\frac{1}{\varepsilon_1} + \frac{d_2}{d_1 + d_2}\frac{1}{\varepsilon_2}. \tag{3}$$

For the metal grating with a certain height, it can be regarded as an assembly of a bottom metal substrate that is semi-infinite thick and a top effective anisotropic medium ($\varepsilon_{\text{eff}}^{\square}, \varepsilon_{\text{eff}}^{\perp}$) of a finite thickness (equal to the grating height). It is anticipated that this equivalent process alters the problem very negligibly and provides a deep insight how the plasmonic element influences the absorption of light in the active layer.

3. Structure and method

OSCs with an inverted structure are more stable than the corresponding devices with a regular configuration [28], and exhibit efficient charge collection at the organic/electrode interface in the cells, due to the removal of the unfavorable interfacial exciton dissociation [3, 29]. Suppression of the metal oxide subgap states in the inverted OSCs significantly improves the charge extraction and performance reproducibility [30]. Here, we consider an inverted OSC structure due to the advantages of efficient charge collection, power conversion efficiency and operation stability over that of the conventional configuration OSCs [3, 28–30]. The planar control device has a configuration of glass/indium tin oxide (ITO)/zinc oxide (ZnO)/poly[[4,8-bis[(2-ethylhexyl)oxy]benzo[1,2-b:4,5-b']dithiophene-2,6-diyl][3-fluoro-2-[(2-ethylhexyl) carbonyl]thieno[3,4-b]thiophene-4,6-diyl]](PTB7): [6, 6]-phenyl-C_{70}-butyric-acid-methyl-ester ($PC_{70}BM$)/Ag, as shown in Fig. 1(a). ZnO-modified ITO works as the cathode. A 3.0 nm thick MoO_3-modified Ag acts as the anode for efficient hole extraction in the inverted OSCs. In our optical simulation, for simplicity, the ultrathin MoO_3 interlayer is not included and the active material is in contact with the Ag anode. Light is normally incident from the glass/ITO side and the reflection loss at the air/glass interface (which can be calculated according to the Fresnel equation) is not considered in this work. The thickness of the ZnO (10 nm)-modified ITO cathode is 180 nm while the 200 nm thick opaque Ag anode is to reflect light. The thickness of the PTB7:$PC_{70}BM$ active layer is denoted by T, fixed as 40 nm unless otherwise described. A thin active layer is studied as a focus because it is

Optics EXPRESS

concluded in our previous work [17] in which case the absorption enhancement factor with respect to the planar control is significant.

Figure 1(b) shows the configuration of the plasmonic OSC when the opaque anode is embossed with a short-pitch grating in sub-hundred nanometer scale. The period, width and height of the grating are denoted by *P*, *W*, and *H*, respectively. As presented in Section II, the interspersed region including alternating Ag and PTB7:$PC_{70}BM$ blend layer can be modeled as a layer of an anisotropic medium, named as effective-medium. The anisotropic permittivities of the effective-medium varies when the duty ratio of the grating changes according to the Eqs. (2) and (3). Here, when Ag and PTB7:$PC_{70}BM$ are defined as material 1 and material 2, respectively, d_1 and d_2 are the widths of the Ag wall (*i.e.*, *P*-*W*) and the PTB7:$PC_{70}BM$ wall (*i.e.*, *W*), respectively. Figure 1(c) shows the equivalent configuration of the plasmonic OSC based on the effective medium analysis. The device turns into a planar form of glass/ITO/ZnO/PTB7:$PC_{70}BM$/effective-medium/Ag. The effective-medium labeled as Part B has a height of *H*. In the equivalent model, the thickness of the active layer decreases by the height of the grating, and the flat Ag plate excludes the grating part. Here, we label the active layer on top of the effective-medium as Part A and the Ag plate below the effective-medium as Part C. In Fig. 1(b), for the real problem, one can easily find the regions corresponding to Part A, B, and C, respectively.

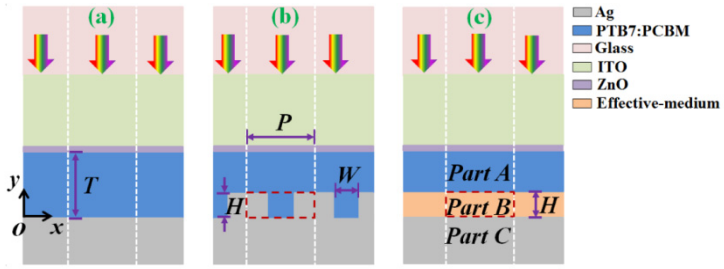

Fig. 1. (a-b) Configurations of the planar device and that embossed with a metal grating at the backside of the active layer. The geometrical parameters of the active layer thickness and the grating profile are as denoted. (c) The equivalent model when the interspersed region is replaced by an effective-medium layer with a thickness equal to the grating height. The interested parts are labeled by Part A, B and C as shown.

In the simulation, the frequency dependent complex permittivities of each layer in the OSC system were derived from the wavelength dependent complex refractive indices measured using the variable angle spectroscopic ellipsometry, and the corresponding optical constants of Ag are taken from the literature [26]. The calculations were carried out by the finite element method (FEM) [17, 18]. Boundary conditions of perfectly matched layer are applied along *y*-axis to eliminate any artificial boundary reflections. Only one unit cell is necessary to be simulated and periodic boundary conditions are applied along *x*-axis. The investigated wavelength range is from 350 nm to 900 nm. The absorption efficiency at a certain wavelength denoted by *Abs* can be directly retrieved once the distribution of the magnetic □eld is calculated out. Only the device performance at TM polarization (with the magnetic field perpendicular to the incident plane) is investigated through this study since there are no plasmonic resonances excited at TE polarization. In order to terminate the polarization sensitivity, one can make the grating into two dimensional arrays.

4. Absorption enhancement based on the effective medium theory

For the inverted OSCs analyzed in this study, the incorporation of a short-pitch metal grating at the silver electrode side helps to significantly improve the absorption in the active layer, similar as in the conventional OSC with ITO as the anode. In Fig. 2(a), the solid line shows the absorption spectrum of the active layer (PTB7:$PC_{70}BM$) in the OSC with the grating

Optics EXPRESS

(shorten as the grating cell). The geometrical parameters are T = 40 nm, P = 20 nm, W = 10 nm, and H = 32 nm. For a fair comparison, a planar control cell, of which the volume of the active material is maintained the same as that of the grating cell (i.e., with T = 24 nm), is simulated, with the absorption spectrum of the active layer indicated by the thin line in Fig. 2(a). One can observe that light absorption in the active layer for the grating cell is enhanced evidently over a broadband wavelength range from 400 nm to 800 nm, compared with that of the planar control cell. The integrated absorption, calculated using AM 1.5G solar spectrum, for the grating cell is 52.9%, improved by more than two-fold as compared to that of the control cell (16%).

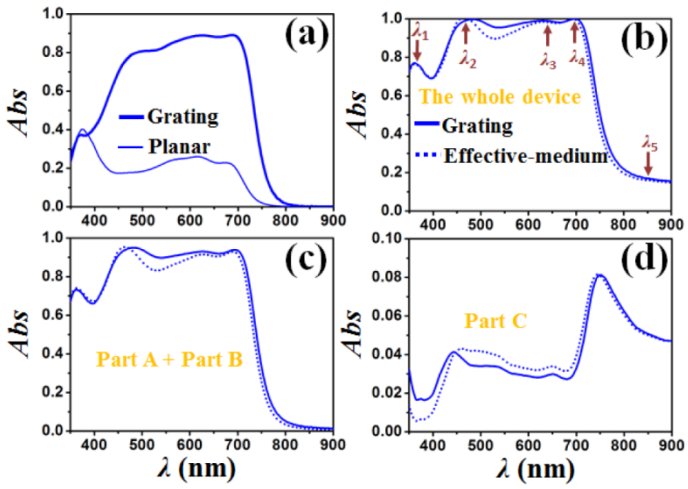

Fig. 2. (a) Absorption spectra of PTB7:$PC_{70}BM$ active layer in the grating cell and the planar cell with the same volume of active material (T = 24 nm). (b-d) Absorption spectra of the whole device, Part A plus Part B, and Part C for the grating cell as well as the effective-medium cell. The geometrical parameters are T = 40 nm, P = 20 nm, W = 10 nm, and H = 32 nm.

In the previous studies [17, 18], we watched over the electric field distributions at the peaks of the absorption enhancement spectrum and found very strong localized electric field is excited within the nanometer-sized groove. Based on the effective medium analysis, in this work, we will provide an alternative understanding on how the short-pitch grating influences the performance of the OSC. Figure 2(b) shows the wavelength-dependent absorption efficiencies of the whole device for the grating cell (solid) and the effective-medium cell (dashed), indicating an excellent agreement with only very minor difference seen at ~550 nm. Moreover, the addition of the wavelength-dependent absorption efficiencies of Part A and Part B regions, and that of Part C also show the same property [as shown in Fig. 2(c) and 2(d)], i.e., the accordance is witnessed in the aspects of curve shape and curve amplitude between the grating and effective-medium cells. The high degree of consistence between the two series of absorption spectra reveals that the effective medium theory is valid for the study of the short-pitch grating incorporated OSC. Given that the wavelengths of the absorption peaks of PTB7:P_{70}CBM do not shift much from those of the whole device, through analyzing the effective-medium device, it is possible to unveil the mechanism of strong and broad absorption in the active layer for the grating cell.

In Fig. 2(b), it is seen that for the whole device, there is a broad and near perfect absorption band between 460 nm and 710 nm along with another peak with relatively less efficient absorption at shorter wavelength. We label the wavelengths at the observed absorption peaks for the effective-medium cell by λ_1, λ_2, λ_3, and λ_4, respectively, as shown in Fig. 2(b); λ_1 = 360 nm, λ_2 = 466 nm, λ_3 = 630 nm, and λ_4 = 700 nm. In addition, another

Optics EXPRESS

wavelength of λ_5 = 850 nm that is out of the PTB7:$PC_{70}BM$ absorption band (with the absorption efficiency for the whole device of only ~15%) will also be studied for elucidating the mechanism. Figures 3(a) and 3(b) displays the field distributions of $|H_z|$ (normalized by the intensity of incident magnetic field) for the grating cell and the effective-medium cell, respectively, at the specified wavelengths. It is seen clearly that at all wavelengths, the magnetic field distributions for the grating cell and the effective-medium cell are very similar to each other, further declaring the validity of using the effective medium analysis in the short-pitch incorporated OSC.

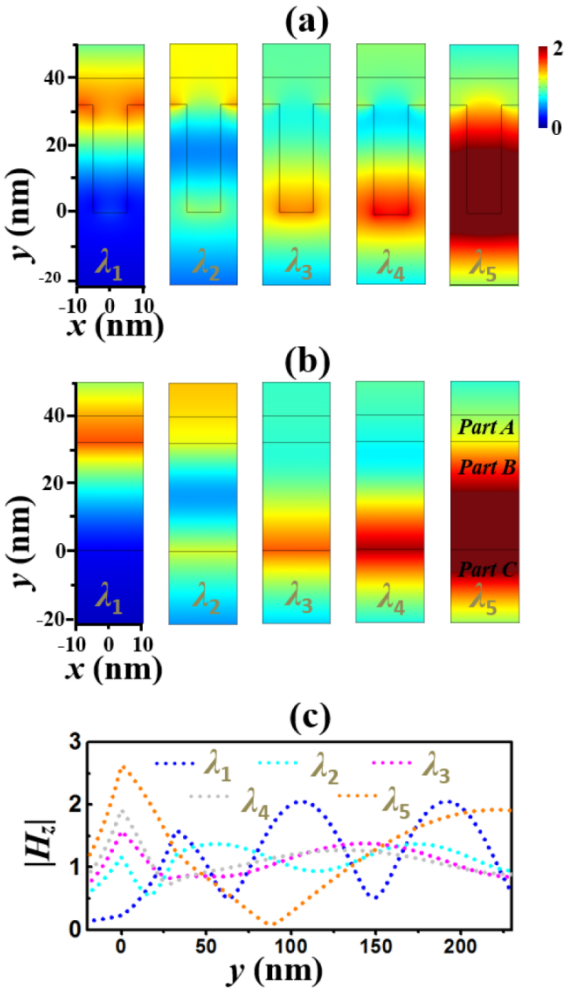

Fig. 3. Distributions of the magnetic field $|H_z|$ for the grating cell (a) and the effective-medium cell (b) at the five specific wavelengths as labeled in Fig. 2(b). (c) The cross-section distributions of $|H_z|$ along y axis for the effective-medium cell at different wavelengths.

At first sight, the field distribution at the first peak differs evidently from those at the other four wavelengths. At λ_1, the incident light hardly reaches the bottom of the active layer (i.e., the bottom of Part B), while at other four peaks, obvious interference fringes are observed at the bottom of the active layer resulting in strong field intensity in both Part B and Part C. Then, the cross-section distributions of $|H_z|$ along y axis at x = -P/2 for the effective-medium cell are also shown in Fig. 3(c). From that, it is clearly demonstrated that at λ_1, the magnetic field is locally maximized at the interface between Part A and Part B, and at other four wavelengths, the position with the maximal field intensity turns to be the interface

Optics EXPRESS

between Part B and Part C. The magnetic field distributions tell that Part B exhibits the metal property at λ_1 as light can hardly penetrate into this layer and at other four wavelengths Part B instead possesses the dielectric property. We then checked the dielectric permittivities at these wavelengths and find out the cause of the distinction. As light is normally incident, only the dielectric permittivities along the interface between different layers (*i.e.*, *x* axis) appears in the Fresnel equations for calculating the reflection/transmission coefficients. Here, in our models, the perpendicular permittivity of the effective medium is along *x* axis. At λ_1 to λ_5, $\varepsilon_{\text{eff}}^{\perp}$ are $-4.55 + 9.24i$, $7.85 + 4.17i$, $7.10 + 4.68i$, $10.85 + 4.76i$, $7.85 + 4.17i$, and $8.06 + 0.05i$, respectively. Part B is equivalent to a metal plate (or a lossy dielectric plate) when the real part of $\varepsilon_{\text{eff}}^{\perp}$ is negative (or positive). The metal nature of Part B at λ_1 is the cause why light almost stops its propagation after passing through the top surface of Part B. At other four wavelengths, Part B can be regarded as a lossy dielectric (with elevated dielectric permittivity with respect to the active material) and the stop of light propagation happens at the top surface of Part C (the metal flat substrate). The absorption efficiency of the active layer is much lower at λ_1 than those at λ_2 (or λ_3, λ_4) because the active material participates in the light absorption process at λ_1 is far less than those at other wavelengths. At λ_5, though the magnetic field is strong in the active layer, its absorption is very low since this wavelength is out of the PTB7:$PC_{70}BM$ absorption band and the corresponding imaginary part of the perpendicular permittivity of Part B is quite small.

In the traditional absorbing system comprising of multilayers [27], the interference effect due to boundary reflections can produce resonant modes of different orders, yielding multiple absorption peaks which are separate from each other. Different orders of resonances differs in their field profiles; the high the order of resonance, the more the node of the field intensity (the node corresponds to a minimum of the field intensity). As a result, the anti-nodes corresponding to a maximum of the field intensity locate at different positions of the multilayer system at different absorption peaks. However, in the present problem, the interface between Part B and Part C always has the maximum $|H_z|$ at the three absorption peaks of λ_2, λ_3, and λ_4. In addition, the magnetic field intensity is maximal at the metal/dielectric interface, indicating the excitation of propagating surface plasmon (SP) mode. The successful excitation of the SP modes at normal incidence reflects that the dispersion diagram of the SP mode for the present system lies within the light cone, thereby satisfying the momentum matching condition, at the investigated broad wavelength range. It is the excitation of the SP modes enabling the trapping of light into the OSC instead of strongly reflecting back to the incident space. For the real structure, the electric field redistributes in the region of Part B. Based on the boundary condition that $D_{\perp}$ is continuous, the active material with a relative smaller absolute value of permittivity has stronger electric field with respect to the metal (in accordance with the results in our previous work), thereby bringing forward efficient light absorption in the active layer. It is noticed that in the planar cell, the propagating SP mode can also be excited among the investigated wavelength range (not shown) but there is no redistribution of the electric field, thereby the accumulation of electric field in the active layer (an important indicator of efficient light absorption) is absent. It is mentioned that at ~550 nm, the absorption spectra of the grating cell and the effective-medium cell present a minor difference. Here, we see from the magnetic field distribution at λ_2 for the grating cell [Fig. 3(a)] that a local enhancement takes place at the top of the metal ridge while at other wavelengths such field localization is absent. It is derived that this localized SP resonance also contribute to the absorption of the investigated OSC but the influence is very minor, yielding the observed tiny deviation of the two absorption spectra at ~550 nm in Fig. 2(b). Until now, the origin of the absorption enhancement effect in the short-pitch incorporated OSC have been discussed on basis of the effective medium theory and an alternative explanation for the broad band efficient absorption in the active layer is the excitation of propagating SP mode over a broad wavelength range.

Optics EXPRESS

5. Effective medium approximation at tuned geometrical parameters

In this section, the validities of the effective medium approximation for OSCs with changes in the active layer thickness and the geometrical parameters of the grating are examined. In other words, this section is dedicated to find when the effective medium theory fails on the explanation of the investigated OSC. Through this section, the absorption efficiencies are calculated for the whole device. And without specifically mentioned, the geometrical parameters are $T = 40$ nm, $P = 20$ nm, $W = 10$ nm, and $H = 32$ nm.

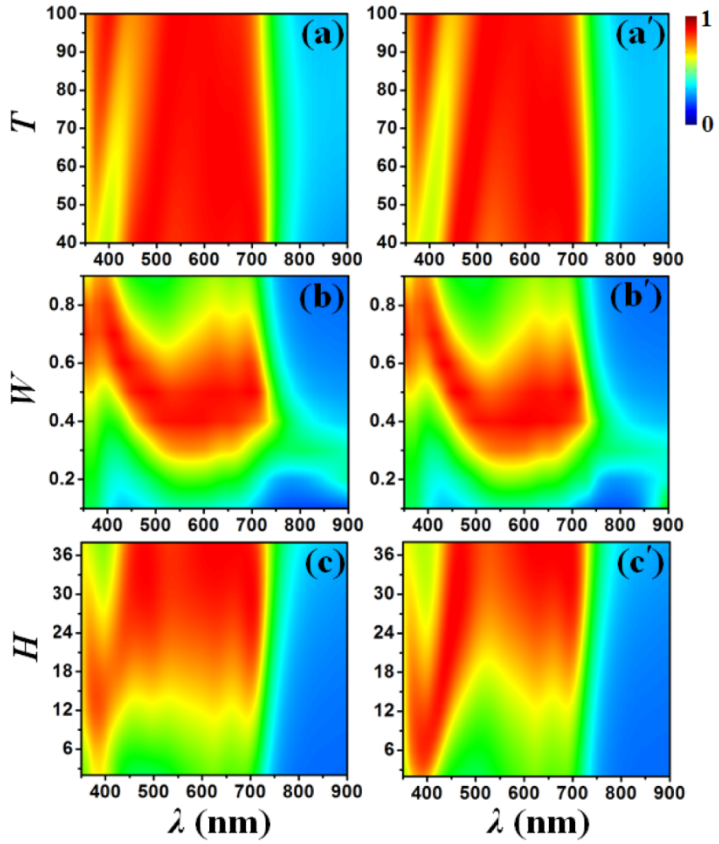

Fig. 4. (a) Contour maps of the absorption for the whole device at varied thicknesses of the active layer, and the grating widths and heights for the grating cell (a-c) as well as the effective-medium cell (a′-c′). Unless otherwise mentioned, geometrical parameters are the same as those in Fig. 2.

First, we study the absorption spectra of the grating and effective-medium OSCs when the thickness of the active layer (T) increases from 40 nm to 100 nm as indicated by the contour map in Figs. 4(a) and 4(a'). It is seen clearly that the two maps have the same profile with each other, reflecting that the effective medium approximation can be applied in this problem no matter the active layer is thin or thick. In addition, one sees that the absorption over the investigated wavelength range reaches an efficient level when the active layer is as thin as 40 nm and the efficiency does not become stronger with increasing T. This is impossible for a planar cell with only cavity modes excited. It reflects that the incorporation of a short-pitch grating enables the OSC become an efficient light trapping element with only a small amount of active material.

In addition, it is expected that the change of width (W) and height (H) of the grating would not lead the effective medium approximation to fail either. The absorption contour maps at

Optics EXPRESS

different W and H are shown in Figs. 4(b), 4(b'), 4(c) and 4(c'), respectively. It is seen that the rule at tuned W is as expected, while at tuned H the law is broken when H is greater than 13 nm. Figures 4(b) and 4(b') indicate that the performance of absorption is optimized when W is around 10 nm, with the duty ratio corresponding to 0.5. Either too little or too much active material degrades the absorption apparently. When W is over small, the equivalent layer (Part B) is close to a metal plate, which leads to two inferior features: the active material participating in absorption is too little and light can hardly penetrates into Part B. For the case with too much active material (i.e., W is approach to P), the effect of the accumulation of the electric field in the active material is weakened according to the volume average theory as presented in Section 2. Therefore, only a moderate W enables not only the excitation of propagating SP mode at the interface of Part B and Part C but also the accumulation of electric field in the region of the active layer. We noticed that the absorption performance of the grating cell with shallow metal ridges is better than that of the effective-medium cell. In Fig. 4(c) an extra absorption band at ~500 nm is found when H is greater than 13 nm when compared with the map in Fig. 4(c'). The field distributions tell that the localized SP resonance excited at the metal ridge plays the role of elevating the absorption. Shallow grating can hardly excited localized SP resonances. Only the grating with sufficiently large height can excited the localized SP resonance, assisting on trapping light as mentioned at λ_2 in Section 4.

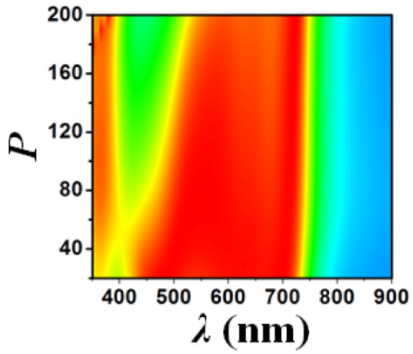

Fig. 5. Absorption spectra for the whole device at varied periods for the metal grating cell.

Finally, we investigate the influence of the grating periodicity on the effective medium approximation as shown in Fig. 5. The investigated period is tuned from 20 nm to 200 nm. It is found that when the period is shorter than 50 nm, the absorption spectrum shows negligible changes from that at P = 20 nm, indicating the reliability of the effective medium analysis on condition that $P << \lambda$. However, when the period is longer than 50 nm, with increasing period, the absorption band at the visible range becomes narrower and narrower though the absorption at the short wavelength range is stronger, resulting in the overall performance of the OSC much poorer. It is noted that for cases with long period gratings, the width and height of the grating should be re-optimized to excite strong plasmonic waveguide modes which might enhance the absorption as reported in Ref. [5].

6. Summary and outlook

In conclusion, we have demonstrated that in a short-pitch metal grating incorporated inverted OSC, the absorption enhancement in the active layer can be explained based on the effective medium theory by regarding the interspersed region with metal and active material as an anisotropic medium. The calculation reveals the absorption spectra of the effective-medium cell approximately consist with those of the proposed grating device when P is far shorter than the investigated wavelength. Magnetic field distributions of the effective-medium cell reflect that at the absorption peaks in the wavelength range longer than 400 nm, propagating

Optics EXPRESS

SP modes are excited at the interface of the effective medium and the bottom metal plate, therefore reducing the reflection apparently. Moreover, the accumulation of the electric field is produced in the grooves filled with the active material according to the volume average theory, which guarantees the observed strong absorption of light. It is shown that the effective medium approximation is insensitive to the thickness of the active layer and the width of the metal ridge. In addition, we have found localized SP resonances can also be excited at the metal ridges, which slightly influences the absorption process in the OSC. For example, we find that at the provided geometrical parameters, there is an extra absorption band at ~500 nm when the grating is higher than 13 nm. Experimentally, the short pitch grating can be easily made from anodic aluminum oxide template or by the nano-imprinting technology [31]. This work contributes to understanding the physical mechanism of plasmonic OSC and the development of high efficiency OSCs.

Funding

National Natural Science Foundation of China (NSFC) (61475109, 61274056, 61275037); Key Research and Development (International Cooperation) Program of Shanxi (201603D421042); Hong Kong RGC (AoE/P-02/12); Young Talents Program of Shanxi Province; Young Sanjin Scholars Program of Shanxi Province; the Outstanding Youth Funding at Taiyuan University of Technology.